Model-Free Closed-Loop Stability Analysis: A Linear Functional Approach

Adam Cooman, *Student Member, IEEE,* Fabien Seyfert, Martine Olivi, Sylvain Chevillard and Laurent Baratchart

arXiv:1610.03235v1 [cs.SY] 11 Oct 2016

***Abstract*—Performing a stability analysis during the design of any electronic circuit is critical to guarantee its correct operation. A closed-loop stability analysis can be performed by analysing the impedance presented by the circuit at a well-chosen node without internal access to the simulator. If any of the poles of this impedance lie in the complex right half-plane, the circuit is unstable. The classic way to detect unstable poles is to fit a rational model on the impedance. This rational approximation has to deal with model order selection, which is difficult in circuits with transmission lines.**

In this paper, a projection-based method is proposed which splits the impedance into a stable and an unstable part by projecting on an orthogonal basis of stable and unstable functions. Working with a projection instead of a rational approximation greatly simplifies the stability analysis. When the projection is mapped from the complex plane to the unit disc, the projection boils down to calculating a Fourier series. If a significant part of the impedance is projected on the unstable part, a low-order rational approximation is fitted on this unstable part to find the location of the unstable poles.

***Index Terms*—Local Stability Analysis, Hilbert spaces**

FREQUENCY domain simulation methods, like Harmonic Balance (HB) or a DC analysis, impose a structure on the obtained solution of the circuit [1]. The DC analysis only allows for a fixed solution, while HB imposes a frequency grid. Any circuit solution that requires more than the imposed frequencies, e.g. an extra oscillation not on the imposed grid, cannot be represented in the constrained frequency grids of DC and HB. The simulator will still find a valid solution, but the obtained orbit will be locally unstable: it cannot recover from small perturbations and will be physically unobservable in the circuit [2]. It is therefore necessary to perform a local stability analysis on each of the circuit solutions obtained with a DC and HB analysis [1].

Over the years, several methods have been developed to determine the local stability of a circuit solution. Some techniques, like the analysis of the characteristic system [2], require access to the simulator. Open-loop techniques, like the analysis of the normalised determinant [1], require access to the intrinsic device models. These classic techniques are therefore hard to implement in commercial simulators.

Closed-loop stability analysis methods can easily be applied as a post-processing step without any internal knowledge of the circuit and can be used in commercial simulators. This is the reason why they have attracted a large interest lately [1], [3], [4]. A closed-loop local stability analysis analyses the linearisation of the circuit around the orbit to determine the stability of that orbit. If the linearised circuit has poles in the complex right half-plane, the orbit is unstable.

The poles of the linearisation around the circuit orbit cannot be obtained directly. Instead a Frequency Response Function (FRF) of the linearised circuit is obtained with small-signal simulations on a discrete set of frequencies. The closed-loop stability analysis then verifies whether the underlying FRF has any poles in the complex right half-plane. All FRFs in the circuit have a common denominator [5]–[7], so it isn't really important which FRF is used in the analysis, as long as the unstable poles are observable in one of the chosen FRFs. To avoid missing an instability in the circuit, many different FRFs can be analysed one-by-one to minimise the risk of not observing a critical pole. Having a fast method to determine stability of a single FRF is therefore critical to a robust stability analysis.

In a pole-zero stability analysis, a rational approximation is fitted on the FRFs. If the rational approximation contains poles in the complex right half-plane, the solution is unstable. Pole-zero identification for stability analysis has to deal with the classic issues of fitting a rational approximation on an FRF [8]. Model-order selection of the rational function is a critical step when stability analysis is considered. Over- or under-modelling can lead to the presence of rogue poles in the model that may migrate to the right half-plane. In circuits with transmission lines, the issues stemming from the use of a rational approximation become worse, because distributed circuits can only be modelled exactly with a rational function over a finite bandwidth, and the obtained model is an approximation only. This can influence the stability of the model. In [9], it is shown that the problems can be solved by cutting the frequency band in pieces and using local low-order approximations to model each piece. If an unstable pole is detected, it is verified to be physical by re-modelling again locally around the found location. This algorithm is commercially available in the STAN tool [10].

The fitting of a rational model can be avoided completely in a stability analysis however. In this paper, we propose to use a functional projection instead of a rational approximation to perform the closed-loop stability analysis. The FRF is projected onto the orthogonal basis of stable and unstable functions. If any part of the FRF is projected onto the unstable part, the circuit solution is unstable. The functional projection doesn't require model-order selection and does not encounter issues when distributed circuits are analysed. Once the stable and unstable parts of the FRF are obtained with the projection, a low-order rational approximation of the unstable part allows to locate the unstable poles.

Adam Cooman is with ELEC at the Vrije Universiteit Brussels (VUB),Belgium. e-mail: acooman@vub.ac.be.

Fabien Seyfert, Martine Olivi, Sylvain Chevillard and Laurent Baratchart are with APICS at INRIA, Sophia Antipolis

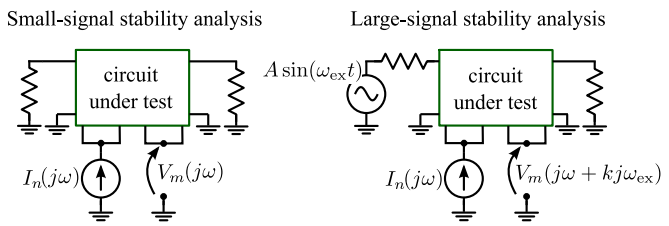

Figure 1. A Small-signal current source is connected to a well-chosen node in the circuit under test to perform the local stability analysis.

The following of the paper is structured as follows: First, the simulation set-up used to determine the FRF of the linearised circuit is discussed (Section I). Then, the details of the functional projection are provided (Section II). In Section III, the method is applied to four examples: First, an artificial example is considered. Then, the small-signal stability of two amplifiers is investigated and finally, the method is applied to investigate the large-signal stability of a circuit.

I. Determining the frequency responses

In this paper, the (trans)impedance presented by the circuit to a small-signal current source will be used as FRF (Figure 1). The small-signal current source is placed in parallel with the circuit and connected to a well-chosen node. It is recommended to choose a node close to the active device(s) in the circuit. The FRF of the linearised circuit is then obtained by first placing the circuit in the required orbit, using either a DC or HB analysis and running a small-signal simulation around this orbit.

In a small-signal stability analysis, the stability of the DC solution of the circuit is investigated, so the FRF of the linearised circuit is obtained with an AC simulation. The impedance of the circuit is then obtained as:

$$Z_{mn}(j\omega) = \frac{V_m(j\omega)}{I_n(j\omega)} \tag{1}$$

where $I_n(j\omega)$ is the small-signal current injected into the selected node n and $V_m(j\omega)$ is the voltage response of the circuit measured at node m in the circuit.

In a large-signal stability analysis, the stability of a large-signal solution of the circuit is investigated. The circuit is driven by a periodic continuous-wave excitation at a pulsation ω_{ex} and the circuit solution is obtained with a HB simulation.

The FRF of the linearised system around the HB orbit is obtained with a mixer-like simulation[1]. As the small-signal will mix with the large signal, several transfer impedances with a different frequency translation are obtained:

$$Z^{[b]}_{mn}(j\omega) = \frac{V_m(j\omega + bj\omega_{\text{ex}})}{I_n(j\omega)} \quad b \in \mathbb{Z} \tag{2}$$

The stability analysis now needs to determine whether the obtained impedances have poles in the right half-plane. The stability analysis of a large-signal orbit doesn't differ much from the analysis of a DC solution [4]. The small-signal stability analysis can be considered a special case where only $Z^{[0]}_{mn}(j\omega)$ is analysed.

[1]In Keysight's Advanced Design System (ADS), this mixer-like simulation is called a Large-Signal Small-Signal (LSSS) analysis.

II. Stable/unstable projection

The projection described here has been used before to perform stable interpolation and extrapolation of FRF data [11]. With slight modifications, it can be turned into a full-blown stability analysis. We first start with a brief introduction to the notion of Hardy spaces.

The Hardy space $H^2(\mathbb{C}^+)$, is defined as the set of all functions g defined on $\mathbb{C}^+$ such that:

- $\forall z \in \mathbb{C}^+$, g is holomorphic at z
- $\sup_{x>0} \int_{-\infty}^{+\infty} |g(x+j\omega)|^2 d\omega < \infty$

A classical result [12] [13] states that every function $g \in H^2$ admits a limiting function $G(j\omega)$ defined on the imaginary axis $j\mathbb{R}$. The latter is obtained by taking the limit of $g(z)$ when z tends non tangentially toward $j\omega$. Moreover $\forall z \in \mathbb{C}^+$, $g(z)$ is equal to the poisson integral of G, that is:

$$g(z = x + jy) = \int_{-\infty}^{+\infty} G(j\omega) \frac{x}{x^2 + (y-\omega)^2} d\omega. \tag{3}$$

The holomorphic nature of g ensures that it is also the Cauchy integral of its boundary value G:

$$g(z = x + jy) = \frac{1}{2\pi} \int_{-\infty}^{+\infty} G(j\omega) \frac{1}{w - z} d\omega. \tag{4}$$

There is a one to one linear correspondence between the Hardy functions g and its boundary value function G. Using this identification, $H^2(\mathbb{C}^+)$ becomes a subspace of the Hilbert space $L^2(j\mathbb{R})$ of square integrable functions on $j\mathbb{R}$. A direct consequence of (3) is that $H^2(\mathbb{C}^+)$ is closed in $L^2(j\mathbb{R})$ and therefore admits an orthogonal complement. An important result [12] asserts that, $\left(H^2(\mathbb{C}^+)\right)^\perp = H^2(\mathbb{C}^-)$ where $H^2(\mathbb{C}^-)$ is defined exactly as $H^2(\mathbb{C}^+)$ above by replacing $\mathbb{C}^+$ by $\mathbb{C}^-$ and taking the supremum over $x < 0$. We therefore have that

$$L^2(j\mathbb{R}) = H^2\big(\mathbb{C}^+\big) \oplus H^2\big(\mathbb{C}^-\big) \tag{5}$$

This decomposition asserts that any square integrable function on $j\mathbb{R}$ decomposes uniquely as the sum of the traces on the imaginary axis, of an analytic function in the right half-plane and a function analytic in the left half-plane. The projection on $H^2(\mathbb{C}^+)$ defines the stable part of the function. The projection onto $H^2(\mathbb{C}^-)$ is the unstable part. As an example, consider P/Q a strictly proper ($\deg(P) < \deg(Q)$) rational function devoid of poles on the imaginary axis. We write its partial fraction expansion as,

$$\frac{P(s)}{Q(s)} = \sum_{i \in I^+} \sum_{k=1}^{k_i} \frac{a_{i,k}}{(s-\lambda_i)^k} + \sum_{i \in I^-} \sum_{k=1}^{k_i} \frac{a_{i,k}}{(s-\lambda_i)^k} \tag{6}$$

where the $\lambda_i' s$ with $i \in I^-$ are poles belonging to $\mathbb{C}^-$, and the ones with $i \in I^+$ belong to $\mathbb{C}^+$. The strict properness of P/Q ensures its square integrability on $j\mathbb{R}$. By unicity its stable part obtained after projection on $H^2(\mathbb{C}^+)$ is found to be,

$$\sum_{i \in I^-} \sum_{k=1}^{k_i} \frac{a_{i,k}}{(s-\lambda_i)^k},$$

while its unstable part is

$$\sum_{i \in I^+} \sum_{k=1}^{k_i} \frac{a_{i,k}}{(s-\lambda_i)^k}.$$

In the general case the projection boils down to calculating certain inner products of $Z_{mn}^{[b]}(j\omega)$ with the basis functions B_k, which form an orthogonal basis of $L^2(j\mathbb{R})$

$$c_k = \left\langle Z_{mn}^{[b]}(j\omega)\,, B_k \right\rangle = \int_{-\infty}^{\infty} Z_{mn}^{[b]}(j\omega)\,\overline{B_k(j\omega)}d\omega \tag{7}$$

$$B_k\left(s\right) = \sqrt{\frac{1}{\pi}}\frac{\left(1-s\right)^k}{\left(1+s\right)^{k+1}} \qquad k \in \mathbb{Z} \tag{8}$$

The overbar $\bullet$ indicates the complex conjugate. All B_k with $k \geq 0$ create a basis for the stable part, while the B_k with negative k form a basis for $H^2(\mathbb{C}^-)$. Once the c_k coefficients are calculated, the stable and unstable parts are easily recovered by calculating

$$Z_{\text{stable}}(j\omega) = \sum_{k=0}^{\infty} c_k B_k(j\omega) \tag{9}$$

$$Z_{\text{unstable}}(j\omega) = \sum_{k=1}^{\infty} c_{-k} B_{-k}(j\omega) \tag{10}$$

The inner product in (7) runs over all frequencies while the impedance function $Z_{mn}^{[b]}(j\omega)$ is only known over a frequency range $\mathbf{f} = [f_{\min}, f_{\max}]$. To impose the finite frequency band on the data, the impedance is filtered before the analysis

$$Z_{\text{f}}(j\omega) = Z_{mn}^{[b]}(j\omega)\,H(j\omega) \tag{11}$$

The filter $H(j\omega)$ is a high-order elliptic lowpass filter with its first transmission zero placed at $f_{\max}$ that imposes band limitation. This filter will stabilise poles close to its cutoff frequency, so $f_{\max}$ should be chosen well beyond the maximum frequency at which the circuit can become unstable. $f_{\min}$ should be placed very close to DC. If $f_{\min}$ can't be close to DC, a bandpass filter should be used for $H(j\omega)$. The filtering ensures that $Z_{\text{f}}(j\omega) \in L^2(j\mathbb{R})$ by suppressing anything outside of the frequency band of interest. The smooth decay to zero of $Z_{\text{f}}(j\omega)$ at the edges of the frequency interval will avoid instabilities to pop up due to the discontinuity of $Z_{mn}^{[b]}(j\omega)$.

In this paper, we always use an elliptic filter of order 10 to filter the data. The passband ripple of the filter is set to 0.1 dB and the stop band attenuation is set to 60 dB. The cutoff frequency of the filter is tuned such that the first transmission zero is located exactly at $f_{\max}$.

A. Transforming to the unit circle

Working with the basis functions defined in (8) is troublesome from a numeric point of view. Performing the projection when working on unit disc yields better results [11]. The mapping from the complex plane to the unit circle is performed with the Möbius mapping visualised in Figure 2:

$$Z_{\text{f}}(s) \underset{\text{Möb}}{\longmapsto} Z_{\text{f}}^{\text{disc}}(z) = \frac{1}{z-1} Z_{\text{f}}\left(\frac{z+1}{z-1} f_{\max}\left(1+\sqrt{2}\right)\right) \tag{12}$$

Our mapping of choice converts square integrable functions on the frequency axis into square integrable functions on the unit circle. Square integrable functions which are analytic on the right half-plane are mapped onto square integrable functions which are analytic inside the unit disc. The basis functions B_k map onto powers of z

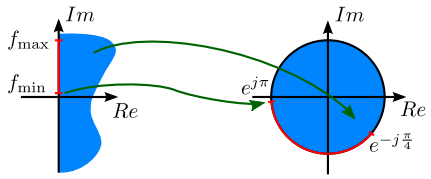

Figure 2. The Möbius transform used in the analysis maps the complex right-half plane to the inside of the unit disc. DC is mapped to -1 and $f_{\max}$ is mapped to $e^{-j\frac{\pi}{4}}$.

$$B_k(s) \underset{\text{Möb}}{\longmapsto} B_k^{\text{disc}}(z) = z^k \tag{13}$$

Projecting on this basis boils down to calculating the Fourier series of $Z_{\text{f}}^{\text{disc}}(z)$, with coefficients given by

$$c_k = \frac{1}{2\pi}\int_0^{2\pi} Z_{\text{f}}^{\text{disc}}\left(e^{j\theta}\right) e^{-jk\theta} d\theta \tag{14}$$

This Fourier series can be calculated in a numerically efficient way using the Fast Fourier Transform (FFT). The FFT requires that the θ-values are linearly spaced between 0 and 2π. Due to the mapping from the complex plane to the unit disc, the samples will not satisfy this constraint. A simple interpolation, using splines, can be used to obtain $Z_{\text{f}}^{\text{disc}}$ on the θ-values required to perform the FFT. The interpolation can introduce artefacts in the unstable part if the FRF is not sampled on a sufficiently dense frequency grid, which will be shown on an example later.

B. Summary of the projection method

The stable and unstable parts of a FRF are determined using the following steps:

1) Multiply the FRF with a high-order filter as in (11)
2) Transform the filtered FRF to the unit disc using (12)
3) Interpolate the transformed FRF to a linear grid and use the FFT to calculate the c_k coefficients
4) Reconstruct the stable and unstable part using (9-10)

When the obtained unstable part is significantly large compared to the stable part, the frequency response is considered unstable.

C. Obtaining the unstable poles

A function is meromorphic on $\mathbb{C}$ if it is holomorphic on $\mathbb{C}$ but on a countable number of isolated poles. The function $\tanh(\omega)$ is for example meromorphic, having infinitely many isolated poles on the imaginary axis placed at $j\pi/2 + jk\pi$ $(\forall k \in \mathbb{Z})$ and being analytic elsewhere. In a small-signal stability analysis of a circuit composed of lumped elements, transmission lines and active devices modelled by negative resistors, the impedances can be shown to be meromorphic functions of the frequency. Under the additional realistic assumption that active elements can only deliver power over

a finite bandwidth, the impedances are proven to possess only finitely many unstable poles in $\mathbb{C}^+$ [5]. Under the generic condition that $Z^{[b]}_{mn}(j\omega)$ is devoid of poles on the imaginary axis, and that the filtering function $H(j\omega)$ decays strongly enough in order to render $Z^{[b]}_{mn}(j\omega)\,H(j\omega)$ square integrable, we conclude that the unstable part of $Z^{[b]}_{mn}(j\omega)\,H(j\omega)$ is a rational function. Its poles coincide with the unstable poles of $Z^{[b]}_{mn}(j\omega)$: note here that the multiplication by $H(j\omega)$ does not add any unstable pole as $H(j\omega)$ is stable. This means that most of the complexity of the frequency response, like the delay, will be projected onto the stable part, while the unstable part can easily be approximated by a low-order rational model to recover the unstable poles.

The 'split-first, approximate later' approach proposed here is therefore more robust than approximating $Z^{[b]}_{mn}(j\omega)$ with a rational model to recover the unstable poles, because we don't have to deal with the issues introduced by trying to approximate the distributed effects in a circuit by a rational model.

Classic rational approximation tools can be used to approximate the unstable part and determine the unstable poles. When multiple frequency responses are analysed simultaneously, a common-denominator approximation is preferred. In our implementation of the method, Kung's method [14], [15] is used to estimate the poles of the unstable part. Alternatively more sophisticated rational approximation engines like RARL2 [16] can be used to recover unstable poles.

III. Examples

The stability analysis will now be applied to four different examples. The first is an artificial example generated in Matlab on which we can demonstrate that the unstable poles in the circuit are recovered perfectly. In the second example, an unstable balanced amplifier is analysed to show that the method works for RF circuits. The third example is a stable circuit where we demonstrate the effects of the filter on the projection method. In the final example, a large-signal stability analysis is performed to verify the stability of a circuit orbit obtained in a HB simulation.

All simulations were performed in Keysight's Advanced Design System (ADS) and the post-processing was performed in Matlab.

A. Example 1: Random state space system

As a first example, the stability analysis is applied to a random system of order 202 generated with the rss function from Matlab. The test system has an unstable pole pair at 1 Hz, as can be seen on its pole-zero map (Figure 3). To introduce delay in the test system, a time delay of 2 s is added to the system.

The frequency response of the system is calculated on 1000 linearly spaced frequency points between 0 Hz and 5 Hz and is shown in green in Figure 4. The obtained stable and unstable parts after projection are shown in red and blue on the same figure.

The obtained unstable part peaks at 1 Hz, which matches the location of the unstable pole pair of the system. Note also that the obtained Z_{unstable} is very simple: it is clearly a second-order system. Most of the complexity of the frequency response, including the delay, is projected onto the stable part. This observation supports the proposed approach of estimating a rational model only after projection. A good fit was obtained with a rational model that consisted of two unstable poles and a single zero. The two poles obtained with a rational approximation of Z_{unstable} coincide exactly with the unstable poles in the circuit as is shown in Figure 3.

The filter in (11) can be used to 'zoom' in on a certain frequency range of the frequency response and isolate a chosen resonance. In a second projection of the same frequency response data, a bandpass filter was used instead of a lowpass filter in the filtering step. The cutoff frequencies of the bandpass filter were 0.7 Hz and 1.3 Hz. The result of the 'zoomed' projection is shown in Figure 5.

B. Example 2: Balanced amplifier

The second example is a balanced amplifier built as a student project for operation around 3.4 GHz (Figure 6). Two BFP520 transistors were used to construct the amplifier. During measurement, the design oscillated around 1.3 GHz when terminated with $50\ \Omega$, so the circuit is a good candidate to verify the proposed method to find the instability in simulations.

The small-signal current source was connected to the collector of the top transistor. The BFP520 has a f_T of 45 GHz, so the maximum frequency for the simulation was set to 50 GHz. The impedance of the circuit was determined starting from DC in 10 MHz steps. The obtained impedance is shown in green in Figure 7, the obtained stable and unstable parts are also shown in the same figure. The instability around 1.3 GHz is detected, but also some artefacts can be observed in the obtained unstable part at higher frequencies. These artefacts are due to the interpolation in step 3 of the stable/unstable projection.

To confirm that the artefacts are indeed artefacts caused by the interpolation, a second simulation was run, but now 1 MHz steps were used instead of 10 MHz. The stable/unstable projection of the denser frequency response data (Figure 8) still predicts the instability around 1.3 GHz, but the artefacts in the unstable part at higher frequencies are gone.

C. Example 3: Stable Low Noise Amplifier (LNA)

In this third example, a stable LNA is analysed to show the effects introduced by simulating the frequency responses on a finite frequency interval only. The LNA under test is described in Infineon application note 051 [17]. The LNA is built around the BFP520 and is shown in Figure 9.

The small-signal stability of the LNA is determined by analysing the impedance presented by the circuit at the collector of the transistor. The impedance was determined up to 10 GHz and shown in green in Figure 10. The result of the stable/unstable projection are plotted in the same figure.

The obtained unstable part of the impedance is very small, but not zero due to the fact that the impedance was only simulated on a finite frequency interval. The filtering smoothens

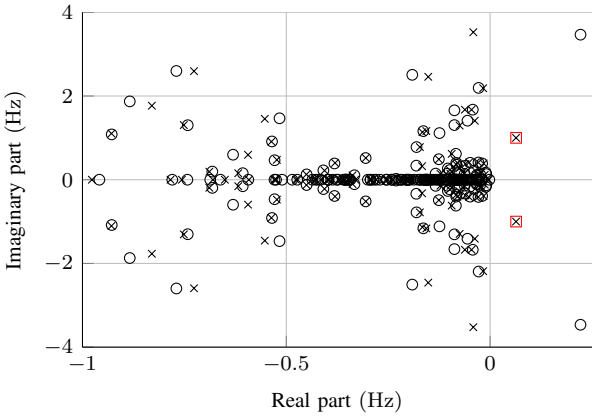

Figure 3. Pole-zero map of the test system. There are 202 poles (×) and 200 zeroes (○). The two poles placed in the right half-plane are easily recovered after the projection by fitting a low-order model on the unstable part (□).

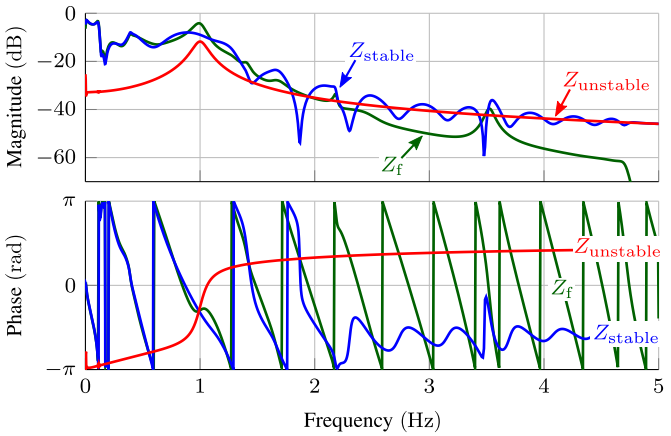

Figure 4. The stable/unstable projection splits the original frequency response (–) in a stable part indicated with (–) and an unstable part indicated with (–)

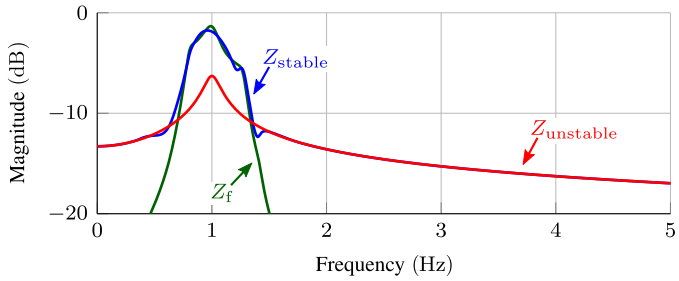

Figure 5. With the filter, it is possible to zoom in on the interesting parts of the frequency response.

the transition to zero at the edge of the frequency interval, but its influence cannot be fully suppressed as is demonstrated by this example.

D. Example 4: R-L-diode circuit

The final example in this paper shows that the stability analysis can also be used to determine the stability of HB simulations of the R-L-diode circuit shown in Figure 11. The circuit is based on [18], but a realistic diode model was used to represent the diode in the circuit instead of the three equations provided in the original paper.

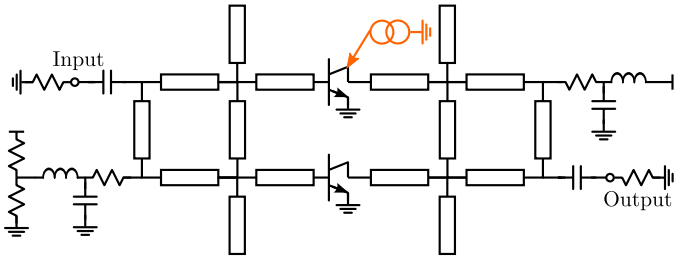

Figure 6. Balanced amplifier was excited at the base of one of its transistors. The full simulation set-up is shown in Figure 14

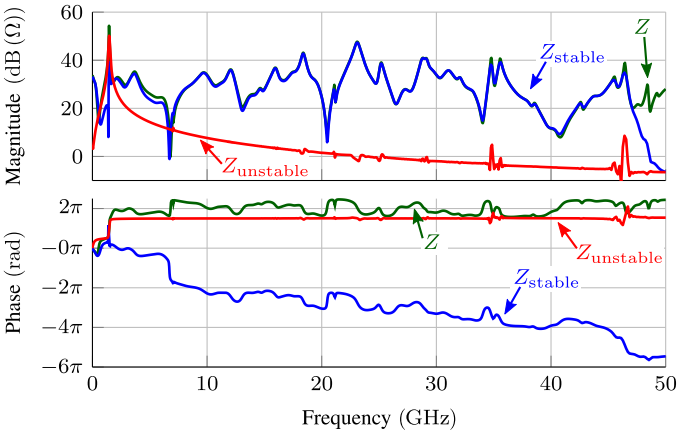

Figure 7. The separation of the impedance (–) into the stable part (–) and unstable part (–) reveals the instability around 1.3 GHz. There are artefacts present in the unstable part due to interpolation of the coarsly obtained impedance data

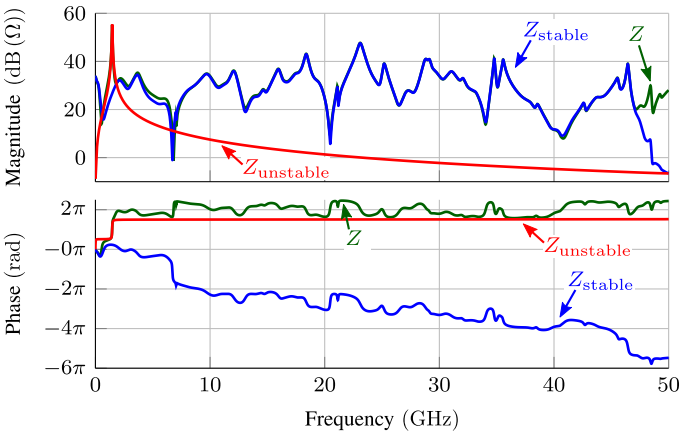

Figure 8. When the impedance of the balanced amplifier is simulated on a finer frequency grid, the artefacts disappear.

The circuit is excited by a single-tone voltage source with an amplitude V_{in} and a frequency of 100 kHz. Because the diode has a transit-time of 4 μs, the circuit generates period-doubling solutions starting from sufficiently high amplitudes V_{in}. For even higher V_{in}, the circuit will create chaotic solutions.

To visualise this behaviour, a bifurcation diagram is constructed using time-domain simulations in the same way as is described in [18]: For every value of V_{in}, 1030 periods of 100 kHz are simulated and the final 30 periods are sampled every $1/100$ kHz. If the circuit solution is periodic with the same period as the input source, all 30 sampled points will fall on top of each-other. If a period-doubling occurs in the circuit, two different values will be obtained.

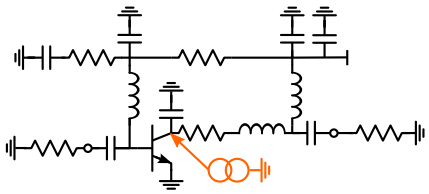

Figure 9. LNA under test built around the infineon BFP520. The impedance small-signal current source is connected to the base of the transistor. The full simulation set-up is shown in Figure 15

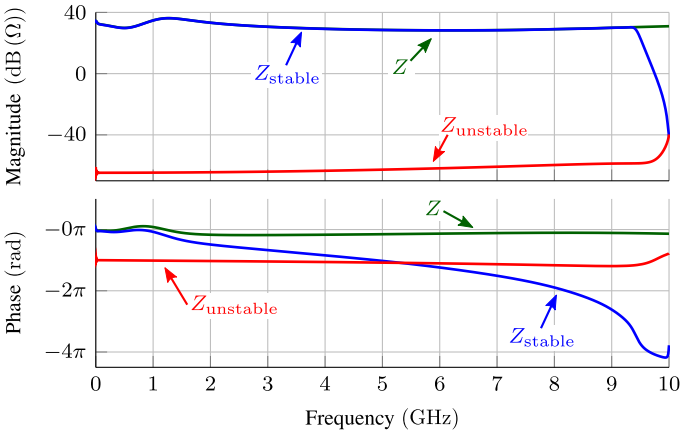

Figure 10. Result of the stability analysis for the stable LNA. The stable part (–) of the projection lies very close to the original impedance (–). The unstable part (–) is very small.

The obtained bifurcation diagram for our R-L-diode example is shown in Figure 12. It is clear that a period-doubling occurs for V_{in} higher than 0.8 V. Starting from 1.8 V the period quadruples. For the highest input amplitudes, a chaotic solution is obtained.

If this R-L-diode circuit is simulated with HB, the circuit solution is constrained to harmonics of 100 kHz. For input amplitudes higher than 0.8 V, where the circuit wants to go to a period-doubling solution, the constrained HB solution will be locally unstable.

We run two HB simulations on this circuit. Both HB simulations have a base frequency of 100 kHz and an order of 10. In the first simulation, V_{in} is set to 0.5 V, which will result in a stable orbit. The second simulation has a V_{in} of 1.5 V, which will cause the orbit to be unstable.

The frequency response of the circuit around the HB solution is obtained with a mixer-like simulation, as explained in the introduction of this paper. The small-signal excitation was swept in both cases on a linear frequency grid starting from (1 kHz + 1 Hz) up to (2 MHz + 1 Hz) in 1 kHz steps. The 1 Hz was added to the start and stop values of the sweep to avoid overlap with the tones of the HB simulation.

The mixer-like simulation in ADS uses Single-Sideband (SSB) current excitations $i(t) = e^{j\omega t}$, which causes the obtained frequency responses $Z'^{[b]}_{mn}(j\omega)$ with $b \neq 0$ to be non-Hermitian:

$$Z'^{[b]}_{mn}(j\omega) \neq \overline{Z'^{[b]}_{mn}(-j\omega)}$$

An alternative representation can make $Z'^{[b]}_{mn}(j\omega)$ Hermitian

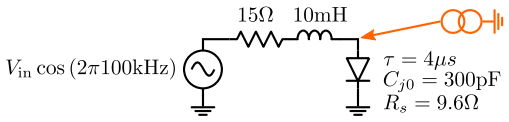

Figure 11. The circuit R-L-diode circuit is excited with a small-signal current source at the diode. The full simulation set-up is shown in Figure 16

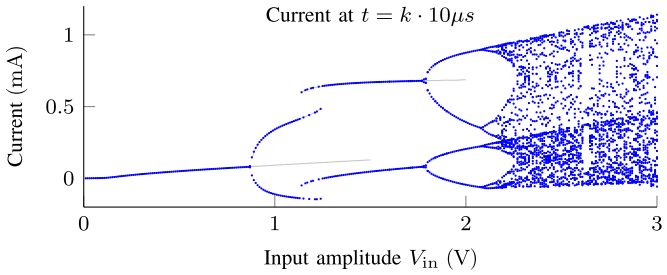

Figure 12. The bifurcation diagram of the R-L-diode circuit shows that a period-doubling occurs for input amplitudes higher than 0.8 V.

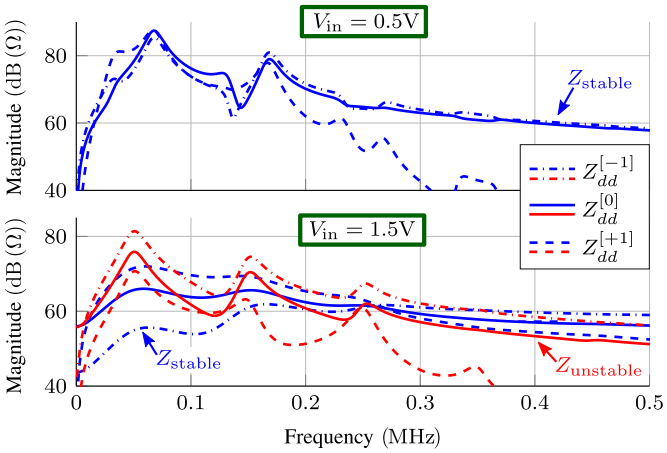

Figure 13. The results of the stability analysis of $Z^{[-1]}_{mn}(j\omega)$ $Z^{[0]}_{mn}(j\omega)$ and $Z^{[+1]}_{mn}(j\omega)$ in the two HB simulations show that, for $V_{\text{in}} = 0.5$ V, the orbit is stable, but for $V_{\text{in}} = 1.5$ V, the orbit is unstable.

by transferring to a sine and cosine basis from the exponential basis [6], [7]

$$Z^{[b]}_{mn}(j\omega) = \frac{1}{2}\left[Z'^{[b]}_{mn}(j\omega) + Z'^{[-b]}_{mn}(j\omega)\right]$$
$$Z^{[-b]}_{mn}(j\omega) = \frac{j}{2}\left[Z'^{[b]}_{mn}(j\omega) - Z'^{[-b]}_{mn}(j\omega)\right]$$

$Z^{[-1]}_{mn}(j\omega)$ $Z^{[0]}_{mn}(j\omega)$ and $Z^{[+1]}_{mn}(j\omega)$ are then analysed with the stable/unstable projection method. The results are shown in Figure 13. The HB solution obtained for $V_{\text{in}} = 0.5$ V is clearly stable: its unstable part is more than 70 dB smaller than its stable part.

In the case for $V_{\text{in}} = 1.5$ V, the solution is clearly unstable as the unstable part lies far above the stable part of the frequency response. Note that the lowest-frequency peak in the unstable part is located around 50 kHz and that copies of the resonance are found at 150 kHz, 250 kHz,... This behaviour is to be expected and indicates that the circuit wants to go to a period-doubling solution.

IV. Conclusion

This paper introduces a closed-loop local stability analysis without using a rational approximation. Instead, the impedance functions are split into a stable and unstable part by projecting onto an orthogonal basis. Transforming the problem to the unit disc allows to calculate this projection with the FFT which makes the projection-based stability analysis very fast. Once the unstable part is obtained, a low-order rational model can be used to find the unstable poles in the circuit.

The proposed method is an elegant way to deal with problems encountered in pole/zero stability analysis of a circuit with transmission lines: no model order selection is required and issues encountered by approximating a distributed circuit with a rational approximation are avoided. The requirements of the projection-based stability analysis are that the frequency responses are sampled on a sufficiently dense frequency grid and that the maximum frequency of the simulations is large enough.

The stable/unstable projection has been successfully applied to both the stability analysis of DC and large-signal solutions of RF circuits.

Acknowlegment

This research was partly supported by the French space agency CNES and partly by the Flemish Agency for Innovation by Science and Technology (IWT-Vlaanderen). We are also thankful to Juan-Marie Collantes (UPV) for fruitful discussions on the topic of closed loop stability analysis.

References

[1] A. Suarez, "Check the stability: Stability analysis methods for microwave circuits," *Microwave Magazine, IEEE*, vol. 16, no. 5, pp. 69–90, June 2015.

[2] A. Suarez and R. Quere, *Stability analysis of nonlinear microwave circuits*. Artech House, 2002.

[3] J. Jugo, J. Portilla, A. Anakabe, A. Suarez, and J. Collantes, "Closed-loop stability analysis of microwave amplifiers," *Electronics Letters*, vol. 37, no. 4, pp. 226–228, Feb 2001.

[4] J. Collantes, I. Lizarraga, A. Anakabe, and J. Jugo, "Stability verification of microwave circuits through floquet multiplier analysis," in *Circuits and Systems, 2004. Proceedings. The 2004 IEEE Asia-Pacific Conference on*, vol. 2, Dec 2004, pp. 997–1000 vol.2.

[5] L. Baratchart, S. Chevillard, and F. Seyfert. (2014) On transfer functions realizable with active electronic components. hal-01098616. Inria Sophia Antipolis. [Research Report] RR-8659.

[6] H. Sandberg, E. Mollerstedt, and Bernhardsson, "Frequency-domain analysis of linear time-periodic systems," *Automatic Control, IEEE Transactions on*, vol. 50, no. 12, pp. 1971 – 1983, dec. 2005.

[7] E. Louarroudi, "Frequency domain measurement and identification of weakly nonlinear time-periodic systems," Ph.D. dissertation, Vrije Universiteit Brussel (VUB), 2014.

[8] R. Pintelon and J. Schoukens, *System Identification a frequency domain approach*, 2nd ed. John Wiley & Sons, Inc., 2012.

[9] A. Anakabe, N. Aylloon, J. Collantes, A. Mallet, G. Soubercaze-Pun, and K. Narendra, "Automatic pole-zero identification for multivariable large-signal stability analysis of rf and microwave circuits," in *Microwave Conference (EuMC), 2010 European*, Sept 2010, pp. 477–480.

[10] AMCAD. engineering, *STAN tool - Stability Analysis*.

[11] M. Olivi, F. Seyfert, and J.-P. Marmorat, "Identification of microwave filters by analytic and rational h2 approximation," *Automatica*, vol. 10, Februari 2013.

[12] K. Hoffman, *Banach spaces of analytic functions*, ser. Prentice-Hall series in modern analysis. Prentice-Hall, 1962.

[13] W. Rudin, *Real and complex analysis*, 3rd ed. New York: McGraw-Hill Book Co., 1987.

[14] S. Kung, "A new identification and model reduction algorithm via singular value decomposition," in *Proceedings of the 12th Asilomar Conference on Circuits, Systems and Computers*, 1978, pp. 705–714.

[15] I. Markovsky, *Low Rank Approximation: Algorithms, Implementation, Applications*. Springer, 2012. [Online]. Available: http://homepages.vub.ac.be/~imarkovs/book.html

[16] J. P. Marmorat and M. Olivi, "RARL2: a Matlab based software for H^2 rational approximation," http://www-sop.inria.fr/apics/RARL2/rarl2.html, 2004.

[17] Infineon, "Application note no. 051; sieget45 low noise amplifier with bfp520 transistor at 1.9ghz," Tech. Rep., 2007.

[18] A. Azzouz, R. Duhr, and M. Hasler, "Transition to chaos in a simple nonlinear circuit driven by a sinusoidal voltage source," *IEEE Transactions on Circuits and Systems*, vol. 30, no. 12, pp. 913–914, Dec 1983.

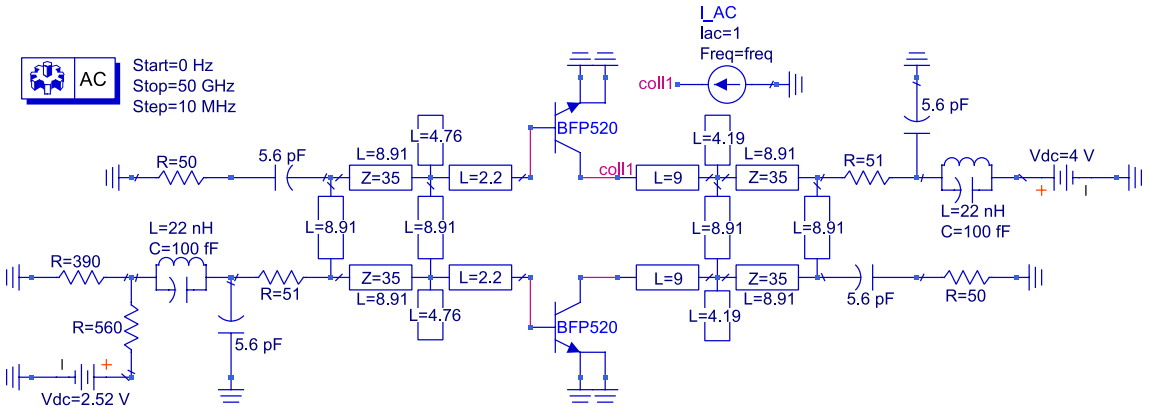

Figure 14. Simulation set-up used to determine the impedance of the Balanced amplifier example. All transmission lines in the circuit are 50Ω lines unless stated otherwise. The length of the transmission lines is given in millimetres. The TLINP model was used for the transmission lines with $\epsilon_r = 6.15$, $\tan(\delta) = 0.003$ and conductor losses $A = 2.5\ ^{\mathrm{dB}}/_{\mathrm{m}}$.

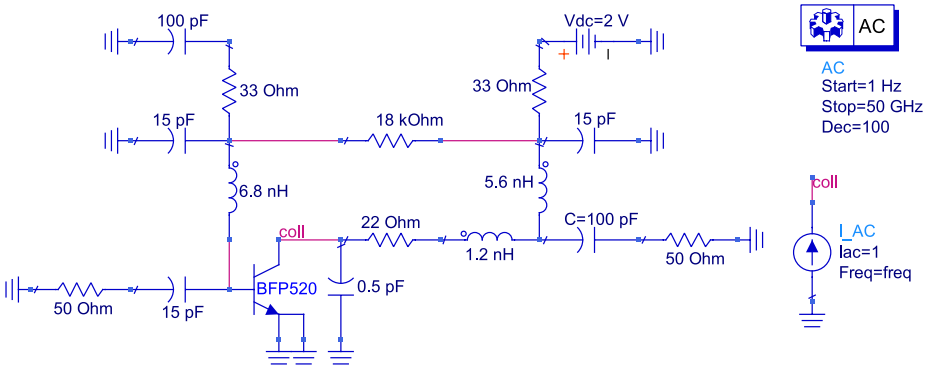

Figure 15. Simulation set-up used to determine the impedance of the LNA example. This is the same circuit as provided in the infineon application node [17]. The model used for the BFP520 is the default model provided by Infineon. The small-signal current source is connected to the collector of the transistor.

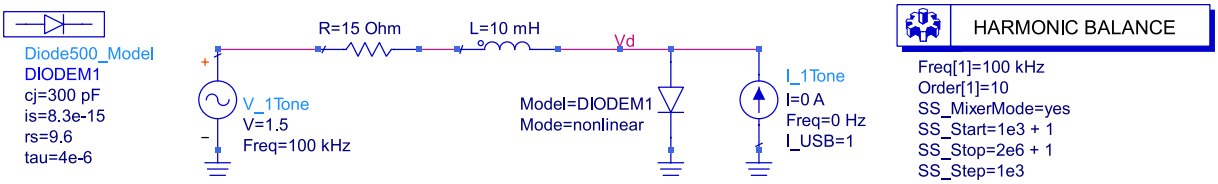

Figure 16. Simulation set-up used to determine the impedance of the R-L-diode example around its HB solution.